ChemComm

Exchange of coordinated carboxylates with azolates as a route to obtain a microporous zinc–azolate framework

Journal:	*ChemComm*
Manuscript ID	CC-COM-02-2022-000925
Article Type:	Communication

COMMUNICATION

Exchange of coordinated carboxylates with azolates as a route to obtain a microporous zinc–azolate framework

Received 00th January 20xx,
Accepted 00th January 20xx

DOI: 10.1039/x0xx00000x

Kira M. Fahy,[a] Mohammad Rasel Mian,[a] Megan C. Wasson,[a] Florencia A. Son,[a] Timur Islamoglu,[a]* Omar K. Farha[a,b]*

Metal–organic frameworks (MOFs) containing open metal sites are advantageous for wide applications. Here, carboxylate linkers are replaced with triazolate coordination in pre-formed Zn-MOF-74 *via* solvent-assisted linker exchange (SALE) to prepare the novel NU-250, within the known hexagonal channel-based MAF-X25 series that has not previously been synthesized *de novo*.

Metal–organic frameworks (MOFs), composed of inorganic nodes and multitopic organic linkers, are highly porous, crystalline materials that have been adopted for many applications including gas storage and separations,[1] sensing,[2] drug delivery,[3] and catalysis.[4] MOFs often offer advantages over other porous materials for such varied applications due to their tunability. The rational design of MOFs through judicious selection of metal node and organic linker combinations allows scientists to leverage their imparted properties for targeted applications. For example, open metal sites (OMS) are selected for by choosing a metal with a preferred coordination number and targeting a topology that results in fewer coordinated ligands.[5] This feature has demonstrated advantages in catalysis as well as gas capture and storage; a coordinatively unsaturated metal site is generally required to bind substrate and/or labile ligands, such as solvent molecules, to initiate a reaction.[5] OMS can additionally induce strong interactions with gas molecules through dipole interactions or charge transfer between the gas molecule and metal cation.[6] One family of MOFs that takes advantage of OMS is the isoreticular series of triazolate-containing frameworks known as MAF-X27, MAF-X25 (MAF = Metal–Azolate Framework), or by the formula $[M(II)_2(OH)_2(BBTA)]$ (M = Mn, Fe, Ni, Cu, Co; H_2BBTA = 1*H*,5*H*-benzo[1,2-d:4,5-d']bis([1,2,3]triazole)).[7–9] These MOFs contain hexagonal channels due to their chain node and adopt an **etb** topology. It is well known that changing the metal comprising the node of a MOF can alter its chemical properties, and thus its potential applications.[10] For example, the Co(II) analogue (MAF-X27) exhibits efficient electrocatalytic oxygen evolution, photocatalytic CO_2 reduction, and selective O_2 chemisorption,[7,8,11] over the Mn(II) analogue (MAF-X25), which shows excellent yet reversible CO_2 capture.[9] While the Zn(II) analogue is hypothesized to be effective for catalysis and CO_2 adsorption due to the bio-inspired Zn–N coordination within the nodes that mimics certain enzyme active sites, researchers have been unable thus far to synthesize this elusive MOF. When mixed *de novo*, Zn(II) and $BBTA^{2-}$ assemble to form the cubic MFU-4 with **pcu** topology[12] rather than the hexagonal MAF-X27.

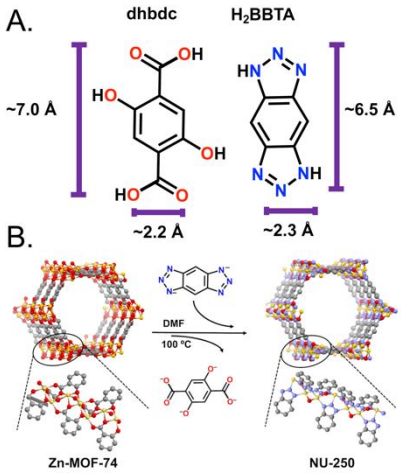

Fig. 1 A) dhbdc and H_2BBTA linker dimensions and B) Schematic of SALE to exchange $dobdc^{4-}$ for $BBTA^{2-}$ in MOF-74. Color key: O (red), N (blue), C (gray), Zn (yellow).

MOFs are most commonly synthesized through solvothermal methods whereby the metal ion or cluster is added in solution with the organic linker and the mixture is heated, typically close to boiling point, for a certain period of time before extensive washing with a solvent.[13] Some MOFs, however, are difficult to synthesize via these *de novo* methods due to the presence of redox active linkers, incompatible functional groups, and/or the inability to isolate kinetic and thermodynamic or intermediate phases.[14,15] Therefore, they must be obtained by post-synthetic modifications on pre-formed MOFs, such as transmetalation,[16] chemical transformations on the linker,[17] solvent-assisted ligand incorporation (SALI),[18] and solvent-assistant linker exchange (SALE), also known as

[a] *International Institute for Nanotechnology and Department of Chemistry, Northwestern University, 2145 Sheridan Road, Evanston, Illinois 60208, United States.*
[b] *Department of Chemical & Biological Engineering, Northwestern University, 2145 Sheridan Road, Evanston, IL 60208, United States.*

Electronic Supplementary Information (ESI) available: [details of any supplementary information available should be included here]. See DOI: 10.1039/x0xx00000x

post-synthetic exchange (PSE).[19] In the latter process, structural linkers from one pre-formed MOF are replaced with the desired linker through a thermodynamically driven equilibrium reaction. Our group and others have demonstrated that SALE is a viable technique to access MOFs that are difficult to synthesize using traditional *de novo* methods.[20,21]

In this study, we utilized SALE to access the Zn(II) analogue of MAF-X27 from the isostructural Zn-MOF-74,[22] also known as CPO-27-Zn or by its formula [Zn_2(dobdc)] (dobdc^{4-} = 2,5-dioxybenzene dicarboxylate).[23] Zn-MOF-74 has been widely studied for gas uptake and storage[24] due to its coordinatively unsaturated metal sites. Although advantageous for gas applications, Zn-MOF-74 lacks high chemical and thermal stability, particularly in water and at high temperatures,[25] due to the weakly coordinated oxygen atom of the deprotonated hydroxyl group of its dobdc^{4-} linker to the Zn site. The oxygen donor atoms, with high electron density, are hard bases while the low-valent Zn(II) is borderline acidic according to Pearson's Hard/Soft Acid/Base (HSAB) classification.[26] The selection of a softer, borderline base ligand, such as a nitrogen-containing triazolate, offers a favorable coordination environment, short metal–ligand distances, and increased Lewis acidity of the metal ions.[27,28] While SALE is most often utilized for linkers with the same coordinating moiety, this is the first instance, to the best of our knowledge, of a linker exchange which incorporates a new functional group coordinated to the node, exchanging a dioxocarboxylate group for a triazolate. The resulting MOF from the SALE experiments, herein referred to as NU-250, was subsequently characterized and the difference in electronic properties of the MOFs were examined with CO_2 uptake studies.

To access the hexagonal **etb** topology for the Zn(II)/H_2BBTA combination, we probed the viability of SALE as a technique to synthesize this elusive MOF (Figure 1). We began by first synthesizing the parent Zn-MOF-74 according to the published literature with slight modifications.[24] Next, we carried out SALE experiments to exchange the dobdc^{4-} linker of MOF-74 with the targeted BBTA^{2-} linker, assuming a defect-free formula to simplify calculations. As previously stated, the softer N-containing azolate was hypothesized to coordinate more favorably to the low-valent Zn(II) ions of the chain node than the hard hydroxy/carboxylate moieties due to a better match of softness according to HSAB theory.

Since H_2BBTA is a strong coordinating ligand to Zn, its concentration as well as synthesis time needed to be optimized to ensure exchange without degradation of the framework. We therefore probed several synthesis conditions including time, temperature, linker ratios, and total solution volume to interrogate the SALE parameter space. First, we tested the addition of a 2:1 theoretical mass ratio of H_2BBTA:dobdc in a solution of MOF-74 in *N,N*-dimethylformamide (DMF), a solvent in which the linker is soluble. After heating for 24 hours at 100 ºC, the mother liquor was decanted, the MOF was washed three times with DMF, and the ^{1}H NMR spectra revealed an exchange of 46%. This process was repeated three more times, and each day resulted in about a 10% increase in BBTA^{2-} linker incorporation, with up to 76% after 96 h (Figure 2). Intending to increase the incorporation further, we then carried out the procedure using a 5:1 mass ratio of H_2BBTA:dobdc monitored over 120 hours. Indeed, after four days, we observed a higher exchange (90%) for the higher concentration, likely due to a greater shift in the equilibrium process favoring BBTA^{2-} incorporation. We elected to move forward with a 96-hour timeframe, as we only observed a 3% increase in linker exchange between the fourth and fifth cycles. We chose to add a 40 mg/mL concentration of H_2BBTA in several cycles as opposed to one cycle in high excess in order to mitigate the formation of side products; potential leaching of Zn(II) ions from the framework would readily react with excess BBTA^{2-} in solution to form the unwanted MFU-4.[12] We also tested H_2BBTA equivalences of 1, 1.5, and 2.5, finding lower exchanges than the 5 eqv. sample for each. We then tested this SALE procedure at temperatures of 80 ºC, 100 ºC, and 120 ºC. While we observed a lower linker exchange after one day with a temperature of 80 ºC, there was negligible difference of linker exchange between samples held at 100 and 120 ºC. Thus, we continued with a timeframe of four days, a linker ratio of 5 eqv. daughter to parent linker, and a temperature of 100 ºC. ^{1}H NMR spectra from three separate trials of the digested MOF after SALE experiments confirmed 85 ± 3.2% exchange of the dicarboxylate linker for H_2BBTA after 4 cycles (Figure S1).

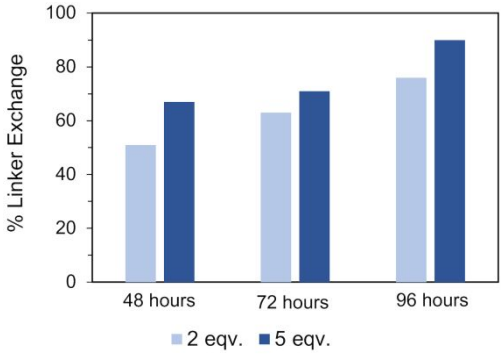

Fig 2. H_2BBTA incorporation into MOF-74 as a function of synthesis time and linker ratio during SALE.

To observe the morphology of the MOF particles, we utilized scanning electron microscopy (SEM). The electron microscopy images revealed the expected hexagonal shape for the starting MOF-74 material (Figure S2). However, the NU-250 particles were less defined when compared to MOF-74. Notably, the absence of well-defined cubic particles in the SEM images further confirms that the unwanted MFU-4 was not formed.

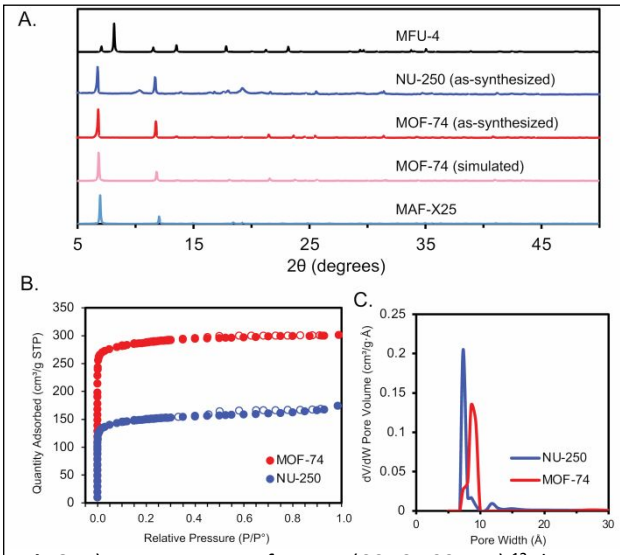

Fig 3. A) PXRD patterns of MFU-4 (CCDC-723714.),[12] the as-synthesized NU-250 SALE product and parent Zn-MOF-74 framework, and simulated MOF-74 and MAF-X25. All spectra are normalized to the sharpest peak. B) Nitrogen adsorption (closed markers) and desorption (open markers) isotherms at 77 K and C) DFT-calculated pore size distributions.

PXRD patterns of the parent framework and resultant SALE product were compared to assess the long-range crystallinity of the material. Figure 3A shows that the **etb** topology of the parent MOF-74 is retained in the SALE product as expected, which also matches the simulated pattern of MAF-X25. Importantly, the PXRD patterns do not indicate the formation of the cubic MFU-4, as evidenced by the absence of the most prominent peaks at 7.1 and 8.1° 2θ. A broad peak around 11° 2θ with low intensity appeared in NU-250 which was absent in the simulated and experimental patterns of MOF-74. The peak originates along the *101* (hkl) plane direction which intersects the metal site and coordinating solvent molecule.[29] More precisely, the peak often appears when solvent is coordinated to metal, though the intensity may be too low to easily observe, as is the case of other MOFs in the MAF-X series. Its presence in NU-250 is likely due to the coordination of large, asymmetric DMF molecules with a thermal vibration. Thus, NU-250 is placed in the MAF-X series with zinc metal ions for the first time where it was previously unable to be prepared *via de novo* method.

Beyond obtaining bulk insights into the linker exchange process, we also used single crystal X-ray diffraction (SCXRD) to obtain atomically precise information about the incorporation of the H_2BBTA linker. We collected and analyzed two kinds of crystals observed in the SEM images—a hexagonal rod and a plate-type particle. In the case of the hexagonal morphology crystal, the dobdc^{4-} linker was observed from X-ray diffraction analysis, indicating the presence of unreacted MOF-74 or a very small amount linker exchange, the latter of which would not be observed *via* SCXRD since MOF-74 is a highly symmetrical framework and we observe only an average structure from this technique. This suggests that the distribution of initial linker exchange is not uniform across the material. The plate-type morphology contains both linkers and crystallizes in a monoclinic *C2/c* space group (Figure S4). Its asymmetric unit contains one Zn ion, one BBTA^{2-}, one dobdc^{4-} linker, and one molecule of DMF (Figure S4C), and is referred to here as NU-251. The Zn ion is tetrahedrally coordinated to two nitrogen atoms from two different linkers of BBTA^{2-}, one carboxylic oxygen atom from the dobdc^{4-} linker, and one oxygen atom of a DMF molecule. The dobdc^{4-} linker coordinates to the metal in an ester fashion and the other oxygen atom of the carboxylic group forms an intra-hydrogen bond with a length of 2.58(4) Å to the hydroxyl group. Four of the six total nitrogen atoms from the two triazolates in each BBTA^{2-} linker are coordinated to four individual Zn ions, leaving two uncoordinated nitrogen atoms within the compact infinite three-dimensional framework. We assumed that this phase forms due to the presence of both BBTA^{2-} and dobdc^{4-} in solution and is stabilized during the formation of the hexagonal framework. Alternatively, it represents a thermodynamically stable second phase which proved difficult to separate from NU-250 by chemical or mechanical methods. The SCXRD data exhibits the complex equilibria of SALE processes which can lend to unexpected products, thus highlighting the importance of thorough parameter screening.

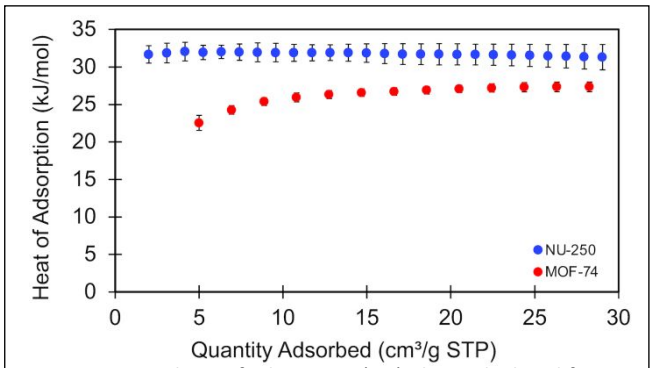

Fig 4. Isosteric heat of adsorption (Q_{st}) plots calculated from CO_2 isotherms at three temperatures (273, 283, 298 K).

Nitrogen isotherms were collected at 77 K for both MOF-74 and NU-250 to measure the porosity of the materials (Figure 3B). The Brunauer-Emmett-Teller (BET) area of MOF-74 measured 1050 m^2/g, slightly higher than the literature values which range from 496-885 m^2/g,[24,30] while NU-250 had a BET area of 575 m^2/g. A decrease in surface area is commonly observed following linker exchange in MOFs[31] and the sample is also assumed to contain a small amount of the aforementioned non-porous 2D sheet phase of the material. Nonetheless, a value of 575 m^2/g confirms that the porosity of the material is largely retained after linker exchange. Density functional theory (DFT) calculated pore size distributions reveal a pore size of around 8.5 Å and 7.5 Å for MOF-74 and NU-250, respectively (Figure 3C), which is expected given the slightly smaller linker dimensions of H_2BBTA compared to dhbdc.

Incorporation of new coordinating moieties to the node can tune the electronic properties of the material. For this system, we utilized carbon dioxide as a probe molecule to investigate the changes to the electronic properties upon exchanging the carboxylate coordination for the N-containing azolate. The design of materials with enhanced interaction with CO_2 has additionally become an increasingly attractive area of research for chemists. A growing concern of atmospheric carbon dioxide levels contributing to global warming warrants development of efficient carbon capture technologies. The low energy requirement of solid sorbents advantages MOFs over other techniques for the removal of CO_2 from flue gas streams.[32] MOF-74 and its isoreticular series are well-known

materials for gas uptake and storage,[24] owing to their coordinatively unsaturated metal sites within its chain nodes. Because of the similar topological features but altered coordination chemistry of the OMS between MOF-74 and the SALE product, we sought to compare their CO_2 uptake capabilities. Overall, MOF-74 showed a higher total uptake of CO_2 than NU-250, which can be attributed to its higher pore volume (Figure S3).

By collecting CO_2 isotherms at multiple temperatures, isosteric heat of adsorption (Q_{st}) can be calculated.[33] Heat of adsorption is a thermodynamic parameter used to screen the strength of the interaction between an adsorbent and an adsorbate. To calculate this for both MOF-74 and NU-250, we collected variable temperature CO_2 adsorption isotherms at 273 K, 283 K, and 298 K. Based on previous work,[9,34] it is hypothesized that both the presence of OMS and the inclusion of N-rich groups within the framework will further enhance CO_2 absorption. Indeed, we observed a maximum Q_{st} for MOF-74 of 27.5 ± 0.7 kJ/mol, which is consistent with reported literature values,[25] while NU-250 achieved a value of 32.2 ±1.1 kJ/mol (Figure 4). Since there is not a significant difference in pore sizes, which have been shown to effect CO_2 adsorption,[35] this increase is attributed to favorable interactions between the gas molecules and the newly incorporated triazolate within the framework of the MOF.

In conclusion, we developed a reproducible method to post-synthetically synthesize the novel MOF NU-250 which has not yet been accessed through *de novo* synthesis. By utilizing SALE, we showed the successful incorporation of a $BBTA^{2-}$ linker into a parent Zn-MOF-74 framework through substitution with the $dobdc^{4-}$ linker. This exchange resulted in the transformation of the coordination sphere from Zn–O bonds from the carboxylate and deprotonated hydroxyl to favorable Zn–N bonds from the triazolate. The resultant material retained bulk crystallinity and porosity. Upon testing CO_2 sorption, it was found that the NU-250 MOF has a higher affinity for the gas than the parent MOF-74 as evidenced by a larger isosteric heat of adsorption, further indicating the tuning of the electronics within the coordination sphere. This work affirms the viability of post-synthetic routes to access MOF topologies that are difficult to attain through traditional *de novo* methods.

Omar K. Farha has a financial interest in NuMat Technologies, a company that seeks to commercialize MOFs.

The authors acknowledge financial support from the Defense Threat Reduction Agency (HDTRA1-19-1-0007) for MOF synthesis and National Science Foundation (NSF) DMREF/GOALI (2119433) for carbon dioxide sorption experiments. This work made use of the IMSERC at Northwestern University, which has received support from the Soft and Hybrid Nanotechnology Experimental (SHyNE) Resource (NSF ECCS-1542205), the State of Illinois, and the International Institute for Nanotechnology (IIN). This work also made use of the Keck-II facility of Northwestern University's NUANCE Center, which has received support from the Soft and Hybrid Nanotechnology Experimental (SHyNE) Resource (NSF ECCS-1542205); the MRSEC program (NSF DMR-1720139) at the Materials Research Center; the IIN; the Keck Foundation; and the State of Illinois, through the IIN. K.M.F. and F.A.S. gratefully acknowledge support from the Ryan Fellowship and the IIN y at Northwestern University. M.C.W. is supported by the NSF Graduate Research Fellowship under grant DGE-1842165. F.A.S. is also supported by the Department of Defense (DoD) through the National Defense Science & Engineering Graduate (NDSEG) Fellowship Program.

Notes and references

1 R.-B. Lin, S. Xiang, W. Zhou and B. Chen, *Chem*, 2020, **6**, 337–363.
2 D. Zhao, K. Yu, X. Han, Y. He and B. Chen, *Chemical Communications*, , DOI:10.1039/D1CC06261A.
3 J. W. M. Osterrieth and D. Fairen-Jimenez, *Biotechnology Journal*, 2021, **16**, 2000005.
4 R. J. Comito, K. J. Fritzsching, B. J. Sundell, K. Schmidt-Rohr and M. Dincă, *J. Am. Chem. Soc.*, 2016, **138**, 10232–10237.
5 Ü. Kökçam-Demir, A. Goldman, L. Esrafili, M. Gharib, A. Morsali, O. Weingart and C. Janiak, *Chemical Society Reviews*, 2020, **49**, 2751–2798.
6 J. S. Lee, B. Vlaisavljevich, D. K. Britt, C. M. Brown, M. Haranczyk, J. B. Neaton, B. Smit, J. R. Long and W. L. Queen, *Advanced Materials*, 2015, **27**, 5785–5796.
7 Y. Wang, N.-Y. Huang, J.-Q. Shen, P.-Q. Liao, X.-M. Chen and J.-P. Zhang, *J. Am. Chem. Soc.*, 2018, **140**, 38–41.
8 A. S. Rosen, M. R. Mian, T. Islamoglu, H. Chen, O. K. Farha, J. M. Notestein and R. Q. Snurr, *J. Am. Chem. Soc.*, 2020, **142**, 4317–4328.
9 P.-Q. Liao, H. Chen, D.-D. Zhou, S.-Y. Liu, C.-T. He, Z. Rui, H. Ji, J.-P. Zhang and X.-M. Chen, *Energy Environ. Sci.*, 2015, **8**, 1011–1016.
10 M. J. Kalmutzki, N. Hanikel and O. M. Yaghi, *Science Advances*, , DOI:10.1126/sciadv.aat9180.
11 X.-F. Lu, P.-Q. Liao, J.-W. Wang, J.-X. Wu, X.-W. Chen, C.-T. He, J.-P. Zhang, G.-R. Li and X.-M. Chen, *J. Am. Chem. Soc.*, 2016, **138**, 8336–8339.
12 S. Biswas, M. Grzywa, H. P. Nayek, S. Dehnen, I. Senkovska, S. Kaskel and D. Volkmer, *Dalton Trans.*, 2009, 6487–6495.
13 O. M. Yaghi, M. O'Keeffe, N. W. Ockwig, H. K. Chae, M. Eddaoudi and J. Kim, *Nature*, 2003, **423**, 705–714.
14 X. Gong, H. Noh, N. C. Gianneschi and O. K. Farha, *J. Am. Chem. Soc.*, 2019, **141**, 6146–6151.
15 A. K. Cheetham, G. Kieslich and H. H.-M. Yeung, *Acc. Chem. Res.*, 2018, **51**, 659–667.
16 K. S. Asha, R. Bhattacharjee and S. Mandal, *Angewandte Chemie International Edition*, 2016, **55**, 11528–11532.
17 S. J. Garibay and S. M. Cohen, *Chemical Communications*, 2010, **46**, 7700–7702.
18 P. Deria, W. Bury, I. Hod, C.-W. Kung, O. Karagiaridi, J. T. Hupp and O. K. Farha, *Inorg. Chem.*, 2015, **54**, 2185–2192.
19 O. Karagiaridi, W. Bury, J. E. Mondloch, J. T. Hupp and O. K. Farha, *Angewandte Chemie International Edition*, 2014, **53**, 4530–4540.
20 F. A. Son, A. Atilgan, K. B. Idrees, T. Islamoglu and O. K. Farha, *Inorg. Chem. Front.*, 2020, **7**, 984–990.
21 M. Kalaj and S. M. Cohen, *ACS Cent. Sci.*, 2020, **6**, 1046–1057.
22 N. L. Rosi, J. Kim, M. Eddaoudi, B. Chen, M. O'Keeffe and O. M. Yaghi, *J. Am. Chem. Soc.*, 2005, **127**, 1504–1518.
23 P. D. C. Dietzel, Y. Morita, R. Blom and H. Fjellvåg, *Angewandte Chemie International Edition*, 2005, **44**, 6354–6358.
24 T. Grant Glover, G. W. Peterson, B. J. Schindler, D. Britt and O. Yaghi, *Chemical Engineering Science*, 2011, **66**, 163–170.
25 H. Yang, F. Peng, C. Dang, Y. Wang, D. Hu, X. Zhao, P. Feng and X. Bu, *J. Am. Chem. Soc.*, 2019, **141**, 9808–9812.
26 R. G. Pearson, *J. Am. Chem. Soc.*, 1963, **85**, 3533–3539.

27 J.-P. Zhang, Y.-B. Zhang, J.-B. Lin and X.-M. Chen, *Chem. Rev.*, 2012, **112**, 1001–1033.
28 L. Feng, K.-Y. Wang, G. S. Day, M. R. Ryder and H.-C. Zhou, *Chem. Rev.*, 2020, **120**, 13087–13133.
29 P.-Q. Liao, X.-Y. Li, J. Bai, C.-T. He, D.-D. Zhou, W.-X. Zhang, J.-P. Zhang and X.-M. Chen, *Chemistry – A European Journal*, 2014, **20**, 11303–11307.
30 H. Kim and C. S. Hong, *CrystEngComm*, 2021, **23**, 1377–1387.
31 S. Jeong, D. Kim, X. Song, M. Choi, N. Park and M. S. Lah, *Chem. Mater.*, 2013, **25**, 1047–1054.
32 A. Ö. Yazaydın, A. I. Benin, S. A. Faheem, P. Jakubczak, J. J. Low, R. R. Willis and R. Q. Snurr, *Chem. Mater.*, 2009, **21**, 1425–1430.
33 A. Nuhnen and C. Janiak, *Dalton Trans.*, 2020, **49**, 10295–10307.
34 A. Demessence, D. M. D'Alessandro, M. L. Foo and J. R. Long, *J. Am. Chem. Soc.*, 2009, **131**, 8784–8786.
35 Z. Cai, C. E. Bien, Q. Liu and C. R. Wade, *Chem. Mater.*, 2020, **32**, 4257–4264.